VEGF Signals Establish Lead Cells that Drive Neural Crest Migration

by Rebecca McLennan[1*], Linus Schumacher[2*], Jason A. Morrison[1], Jessica M. Teddy[1], Dennis Ridenour[1], Andrew Box[1], Craig Semerad[1], Hua Li[1], William McDowell[1], David Kay[1], Philip K. Maini[2], Ruth E. Baker[2], and Paul M. Kulesa[1,3**]

1 Stowers Institute for Medical Research, 1000 E. 50th St, Kansas City, MO, 64110, USA

2 Oxford University, Centre for Mathematical Biology, Mathematical Institute, 24-29 St Giles', Oxford, OX1 3LB, UK

3 Department of Anatomy and Cell Biology, University of Kansas School of Medicine, Kansas City, KS, 66160, USA

*both authors contributed equally to this work, **corresponding author

Abstract

Embryonic neural crest cells travel in discrete streams to precise locations throughout the head and body. We previously showed that cranial neural crest cells respond chemotactically to vascular endothelial growth factor (VEGF) and cells within the migratory front have distinct behaviors and gene expression. We proposed a cell-induced gradient model in which lead neural crest cells read out direction information from a chemoattractant profile and instruct trailers to follow. In this study, we show that migrating chick neural crest cells do not display distinct lead and trailer gene expression profiles in culture. However, exposure to VEGF in vitro resulted in the upregulation of a small subset of genes associated with an in vivo lead cell signature. Timed addition and removal of VEGF in culture showed the neural crest cell gene expression changes were rapid. Model simulations incorporating an integrate and switch mechanism predicted migration efficiency is influenced by behavior switching. We then used tissue transplantation of VEGF-producing cells either adjacent to or within the trailer subpopulation and showed diverted cell trajectories and stream alterations consistent with model predictions. Gene profiling revealed an upregulation of a subset of lead genes in diverted cells that encountered the VEGF. Injection of Np1-Fc into the trailing subpopulation or electroporation of VEGF morpholino to reduce VEGF signaling failed to alter trailer neural crest cell trajectories, suggesting trailers do not require VEGF to maintain coordinated migration. These results indicate that VEGF is one of the signals that establishes lead cell identity and its chemoattractant profile is critical to neural crest cell migration.

Introduction

One of the most striking examples of embryonic cell migration is the pattern of the multipotent, highly invasive neural crest. Neural crest cells exit the dorsal neural tube in a rostral-to-caudal order and are sculpted into discrete streams that stretch throughout the landscape of the developing vertebrate embryo (Theveneau and Mayor, 2013; Kulesa and McLennan, 2015). This widespread migratory pattern results in a contribution from the neural crest to nearly every major organ. As such, a large class of neural crest-related congenital birth defects has been termed neurocristopathies (Cordero et al., 2011; McKeown et al., 2013; Butler-Tjaden and Trainor, 2013; Kulesa et al., 2013). Neurocristopathies may severely affect craniofacial, cardiovascular, and autonomic nervous system function. In addition, neural crest-derived melanoma and neuroblastoma may be very aggressive cancers (Kulesa et al., 2013; Maguire et al., 2015). Thus, the clever invasive ability and significant contribution to organogenesis of the neural crest make this cell population an important model to development and cancer.

Advances in time-lapse imaging in a number of embryo model systems have revealed the complexity of neural crest migratory patterns (Blasky et al., 2014; Clay and Halloran, 2014; McGurk et al., 2014; Moosmann et al., 2014; Kulesa et al., 2013; Nishiyama et al., 2012). Neural crest cells may move collectively in sheets and chains, or as individuals in multicellular streams (McLennan and Kulesa, 2015). Regardless of the type of migration, neural crest cells follow stereotypical migratory pathways in a directed manner and maintain discrete stream integrity. Thus, despite the wide variety of crest

cellular phenomena, persistence, linearity and cohesion are a common thread of neural crest cell migratory patterns.

To more rapidly test hypothetical mechanisms of neural crest cell persistence, linearity, and stream cohesion, computational models have been formulated from empirical data. These models include: (1) frontal expansion (Newgreen et al., 2013); (2) co-attraction/contact inhibition of locomotion (CIL) (Carmona-Fontaine et al., 2011); (3) and cell-induced gradient (McLennan et al., 2012). The frontal expansion model is based on enteric neural crest cell dispersion and proliferation within open spaces of the developing gut (Young et al., 2004; Simpson et al., 2007). Beautiful time-lapse imaging of mouse enteric neural crest cells has revealed that advancing cells move with low directionally and are leap-frogged by trailing cells in a repeating pattern (Young et al., 2014). In contrast, the co-attraction and contact inhibition of locomotion (CIL) model proposes that secretion of a local chemoattractant by migrating neural crest cells prevents widespread dispersal and makes CIL more efficient to generate cell polarity and directed movement (Carmona-Fontaine et al., 2011; Woods et al., 2014). Lastly, we proposed a cell-induced gradient model in which lead neural crest cells respond to a chemotactic guidance signal and instruct trailer cells to follow (McLennan et al., 2012). Together, these models that reflect the diverse characteristics of neural crest cell migratory patterns throughout the embryo are helping to shed light on underlying mechanisms.

The consistent discoveries that chemotactic factors are present within the embryonic microenvironment changed the neural crest cell migration paradigm. These chemotactic factors include glial cell derived neurotrophic factor (GDNF) (Lake and Heuckeroth, 2013), platelet derived growth factor (PDGF) (Eberhart et al., 2008; He and Soriano, 2013), fibroblast growth factors (FGFs) (Sato et al., 2008) and vascular endothelial derived growth factor (VEGF) (McLennan et al., 2010), complement fragment c3a (Carmona-Fontaine et al., 2011), and stromal cell-derived factor 1 (SDF1) (Kasemeier-Kulesa et al., 2010; Saito et al., 2012; Theveneau et al., 2013). This evidence has led to questions about how neural crest cells interpret chemical signals in the microenvironment and from each other to move in a directed manner and migrate as a coordinated population.

We previously showed that VEGF acts as a chemoattractant for neuropilin-1 expressing cranial neural crest cells in chick (McLennan et al., 2010). Loss of neuropilin-1 function caused neural crest cells to stop prior to entering the second branchial arch (McLennan and Kulesa, 2007). Computational modeling then predicted the presence of lead and trailing neural crest cells in the presence of a VEGF chemoattractant profile shaped by tissue growth and cell consumption, which we termed a cell-induced gradient model described above (McLennan et al., 2012). Gene profiling identified distinct expression patterns between lead and trailer neural crest cells (McLennan et al., 2012) that correlated with unique cell behaviors observed within each of these two subpopulations (Teddy and Kulesa, 2004). Interestingly, tissue transplantations that placed trailer neural crest cells in advance of the leaders showed trailers adopted invasive behaviors and

gene expression based on their new stream position (McLennan et al., 2012). Further single cell profiling has now identified a stable and consistent molecular signature unique to a subset of lead cells narrowly confined to the advancing migratory front, which we call trailblazers (McLennan et al., 2015). Whether VEGF is one of the microenvironmental signals that establishes lead and trailer neural crest cells and how cells interpret the VEGF chemoattractant profile to move in a directed manner remains unknown.

Here, we study these questions using the chick embryo model system and agent-based computational modeling. We first compare the gene expression profiles of migrating neural crest cells exiting from neural tube explant cultures to in vivo data. We examine the response of neural crest gene expression to timed addition and removal of VEGF in this assay. Based on this data, we construct an integrate and switch model mechanism and test cell migration efficiency as a function of switching times. To test the neural crest migratory response to alterations in the in vivo VEGF chemoattractant profile, we place ectopic sources of VEGF either adjacent or within the trailing portion of the stream and monitor alterations to cell trajectories, stream integrity, and gene expression. We test whether trailer neural crest cells require VEGF for guidance by morpholino knockdown of VEGF production in the ectoderm or by binding up endogenous VEGF protein within the migratory pathway. Finally, we examine changes in lead neural crest cell gene expression in response to reduction in VEGF signaling either by binding up of endogenous VEGF or knockdown of the neuropilin1 receptor by siRNA.

Materials and Methods

Embryos and in ovo cell labeling and transplants

Fertilized white leghorn chicken eggs (supplied by Centurion Poultry Inc., Lexington, GA) were incubated at 38C in a humidified incubator until the desired HH (Hamburger and Hamilton, 1951) stage of development.

For VEGF transplant experiments, premigratory neural crest were labeled by injecting Vybrant DiO (V22889, Invitrogen, Carlsbad, CA) into the lumen of the neural tube. Embryos were then re-incubated for 12hrs to allow neural crest cells to exit and form a discrete migratory stream. Clumps of DiI-labeled endothelial cells (control (CRL-2279, ATCC, Manassas, VA)) or VEGF-expressing cells (CRL-2460, ATCC) were then transplanted either within or adjacent to (adjacent to rhombomere 3 (r3)) the trailing subpopulation of the migrating neural crest stream. Manipulated embryos were either re-incubated for 1 hr and then mounted on glass bottom dishes (P35G-1.5-20-C, MatTek Corporation, Ashland, MA) for time-lapse imaging as previously described (Chapman et al., 2001; McKinney et al., 2013) or for 12 hrs before being harvested for static imaging and cell isolation for gene expression profiling as previously described (McLennan et al., 2012). For VEGF signaling knockdown experiments, neuropilin-1-Fc (566-NNS, R & D Systems, Inc.) targeted injections and neuropilin-1 siRNA electroporations were performed as previously described (Bron et al., 2004; McLennan and Kulesa, 2007). Control GFP (pMES) or fluorescently tagged VEGF morpholino (GeneTools, Philomath, OR) was targeted to the ectoderm directly overlying the trailing neural crest cell subpopulation by injecting a small amount of construct or morpholino

immediately above the cranial ectoderm on one side of the embryo at HH St 9-11, and then electroporated with platinum electrodes placed either side of the embryo. After 24 hrs re-incubation, embryos were fixed, cryostat sectioned and HNK-1 immunohistochemistry was performed as previously described (McLennan et al., 2010).

In vitro assays

Cranial neural tubes (r1-r7) containing premigratory neural crest cells were cultured in vitro as previously described (McLennan et al., 2010). For the lead/trail analysis, neural tubes were plated on nuclease-free 1.0 PEN Membrane Slides (415190-9081-000, Zeiss, Jena, Germany) so that neural crest cells would migrate onto the slides and be easily and selectively isolated. After 24 hrs of incubation to allow for neural crest migration, slides were dehydrated with 100% ethanol for 5 minutes. Using a PALM Microbeam (Zeiss), neural crest cells adjacent to the neural tube (trailers) and at the edge of the invasive front (leaders) were catapulted without contact into an adhesive cap (415190-9181-000, Zeiss), lysed and used for standard RT-qPCR on an ABI 7900HT Fast Real-Time PCR system (ABI, Oyster Bay, NY). For the time-course exposure to VEGF, neural tubes were plated on glass bottom dishes, one neural tube per dish. After overnight incubation, with Ham's F-12 Nutrient Mix Media (11765054, Invitrogen, Grand Island, NY), neural tubes were removed leaving only neural crest cells. Ham's F-12 Nutrient Mix Media containing VEGF then replaced the plain media for 2 hours, and then the media was replaced with plain media (Fig. 3A). This media was then replaced with media containing VEGF in a temporal manner (Fig. 3A). Neural crest cells were lysed directly on the glass bottom dishes at different time points by

replacing media with 10ul of Cells-to-Ct lysis solution containing 1:100 DNAse I (4387299, Life Technologies-Invitrogen). The lysis reaction was halted, after 15 minutes at room temperature, with 1ul of Stop solution and samples were immediately placed on dry ice and stored at -80C.

Molecular profiling

cDNA was synthesized directly from sample lysates (438814, Life Technologies) in reactions that included 1ul of RNAse inhibitor (N261b, Promega, Madison, WI). Gene-specific targets were pre-amplified from a portion of the cDNA in 20ul preamp reactions using 14 thermal cycles according to a miniaturized version of Life Technologies' Cells-to-Ct preamp kit (4387299, Life Technologies). Pre-amplified products were diluted with 1X TE before being analyzed by microfluidic RT-qPCR on Fluidigm's Biomark HD platform. Non-logarithmic curves were manually removed in Biomark software. Data was normalized using three reference genes chosen from at least 6 candidates and analyzed with Biogazelle's qBASE software. To combat the variability inherent within our model system, we set statistical significance at $p<0.1$, choosing to include rather than exclude potential genes of interest. In lieu of multiple testing correction to eliminate false positives, we focused on genes that were implicated in multiple analyses. Partek's Genomics Suite was employed for generating clusters, dissimilarity matrices and intensity plots.

Fluorescent in-situ hybridization chain reaction (HCR)

Neural tubes were isolated and plated, 5-6 neural tubes per glass bottom dish and incubated overnight described above. Cultures were fixed in 4% paraformaldehyde at room temperature for 1 hr and dehydrated stepwise with an ethanol/PBS-T gradient. Cultures were left overnight in ethanol and then rehydrated stepwise into PBS-T. FoxD3, Hand2 and Bambi mRNA transcripts were visualized simultaneously in neural crest cells in culture dishes placed on the confocal microscope stage and images collected using the same imaging settings for all cultures (LSM 710, Zeiss). HCR probes were used at a concentration of 2 nM and hairpins at a concentration of 30 nM.

Analysis of HCR fluorescence and neural crest cell behaviors

We calculated the intensity analysis of HCR fluorescence in neural tube explant cultures as a measure of gene expression signal. For this analysis, regions of interest were identified either proximal or distal from each explanted neural tube (Fig. 1F). Within the regions of interest, we used the 'Surfaces' function of Imaris (Bitplane USA) to identify cells using the FoxD3 channel and then measured the mean intensity of all fluorescent channels within each surface. The box plots in Fig. 1F were generated by combining the mean intensities from all of the proximal or distal regions of interest. Plus signs indicate outliers, while the box plots and whiskers indicate the quartiles and range, respectively, of each data set

Computational Modeling

To verify that our experimental observations are consistent with our hypotheses, we employ the hybrid computational model first described in McLennan, Dyson et al. (2012), with agent-based representation of cells and a chemoattractant described by a continuous reaction-diffusion equation. Previously, we introduced modifications and improvements to the model, which we further build upon in this work. For the integrate-and-switch mechanism, we introduced a variable recording how much signal each cell had sensed. This variable increases at a fixed rate when a chemoattractant gradient above the sensing accuracy threshold is sensed, and decreases otherwise, at rates inversely proportional to the parameters leader-to-trailer switching time, t_{LF}, and trailer-to-leader switching time, t_{FL}, respectively. Pseudocode and a table of parameters used can be found in the supplementary materials.

To represent transplants of ectopic VEGF, we altered the chemoattractant distribution in our model simulations. From t = 12 hours (6 hours after the start of migration), the background chemoattractant production was increased in a subregion of the migratory domain. To represent placement of a VEGF source outside of the domain (adjacent to the stream), the chemoattractant production was increased in a thin strip of $1/20^{th}$ the width of the domain, and for placement within the stream, a region of half the domain-width was chosen. In both cases, the length of the transplant was $1/8^{th}$ of the domain length, and increased with domain growth.

Results

Lead and trailer molecular profiles vary according to the embryonic microenvironment and do not exist in vitro

Using morphometric analysis and molecular profiling, we have previously shown that neural crest cells within a stream display different phenotypes and genotypes: in particular, a stream is composed of at least two subpopulations, leaders and trailers (McLennan et al., 2012; Teddy and Kulesa, 2004). Here, we conducted experiments where, as far as possible, the influence of the microenvironment was removed to address whether these subpopulations are predetermined or regulated by the surrounding embryonic microenvironment. We excised neural tubes containing premigratory neural crest cells, allowed the neural crest cells to migrate out from the neural tubes in vitro and isolated cells from the invasive front (distal) and near the neural tube (proximal) to perform molecular profiling (Fig. 1A). Euclidean clustering showed that lead and trailing molecular profiles seen in vivo are drastically different to those seen in vitro (Fig. 1B). A Euclidean dissimilarity matrix intensity plot shows that in vitro trail and in vitro lead were the most similar to each other (7.5) while in vitro lead and in vivo lead were the least similar to one another (16.8) (Fig. 1C). It is important to note that even though the in vitro samples were most similar to each other, they were still very different from one another (score of zero meaning the same) (Fig. 1C).

When the molecular profiles were compared at the individual gene level, there were 11/84 genes that were upregulated in the lead for both in vitro and in vivo, but only one gene, RUNX2, that was upregulated in both (Fig. 1D). There were 9/84 genes

upregulated in the trail in vivo and 5/84 genes upregulated in the trail in vitro but only one gene, FOXD3, that was expressed at high levels in both (Fig. 1E). Thus, even though there were gene expression profile differences in vitro between cells at the invasive front compared to cells near the explanted neural tube, these profiles did not reflect the lead and trailing neural crest cell gene expression profiles we determined in vivo (McLennan et al., 2012)

To confirm our in vitro profiling results by expression analysis, we used fluorescent in-situ hybridization chain reaction (HCR) methodology to simultaneously observe HAND2, BAMBI, and FOXD3 in migrating neural crest cells (Fig. 1F). We found that FOXD3 was strongly expressed in migrating cells near the explanted neural tubes (Fig. 1G, red). In contrast, expression of HAND2 and BAMBI was very low throughout the entire migrating neural crest cells in vitro (Fig. 1G, green and yellow). Therefore, gene expression analyses by HCR agreed with our in vitro RT-qPCR profiling results and confirmed no lead/trailing molecular signatures in vitro.

To investigate whether VEGF exposure in culture could influence the gene expression profile of migrating neural crest cells, we added VEGF to neural tube cultures overnight (Fig. 2A). Euclidean clustering and Euclidean dissimilarity matrix intensity plots showed that upon exposure to VEGF lead and trailing gene profiles in vitro were still very different to the lead and trail molecular signatures measured in vivo (Fig. 2B, C). Exposure to VEGF in lead neural crest cells in vitro significantly induced the expression of 14 genes examined (Fig. 2D). Of these 14, 9/14 were up- and 5/14 were down-

regulated, compared to in vitro lead neural crest cells not exposed to VEGF (Fig. 2D). Three of the genes that were upregulated are genes typically associated with the most invasive in vivo lead neural crest cells; NEDD9, BAMBI and NOTCH1 (Fig. 2D, purple). These experiments reveal that lead and trailing neural crest cell molecular signatures are an emergent property after exposure to signals within the embryonic neural crest microenvironment, one of which is VEGF.

Neural crest genes are rapidly induced in vitro in response to changes in VEGF

Tissue transplantations we previously performed in vivo (McLennan, Dyson et al., 2012) showed that neural crest cells altered their gene expression profiles to correspond with new stream positions. We revised our computational model to reflect this, but it has remained unclear how rapidly neural crest cells could alter their expression profile and thus transition from a lead to trailing cell behavior or vice-versa. To determine the gene expression dynamics of neural crest cells to addition or removal of VEGF in culture, we performed a series of timed experiments. That is, neural tube cultures were exposed to VEGF for 2 hrs, then VEGF was removed for 90 min and re-applied for 90 min (Fig. 3A). Samples of neural crest cells for RNA isolation and profiling were taken at a non-linear set of specific time points (Fig. 3A). When the temporal expression of all genes was examined, we found that 17/25 and 9/25 showed a consistent change in expression within the first 4 minutes after removal and re-addition, respectively (Fig. 3B, C).

After the initial exposure to VEGF for two hours, 18 genes were significantly downregulated (Table 1). No genes in our set were significantly upregulated. When

viewing response time of genes to both removal and reapplication of VEGF, many genes responded to removal of VEGF within four minutes, but then the response to reapplication of VEGF of those same genes varied greatly (Fig. 3C). Of the 18 genes, 14 genes had reoccurring responses upon removal and/or reapplication of VEGF. Six genes were significantly downregulated upon exposure to VEGF and then upregulated after removal of VEGF but no significant change upon the reapplication of VEGF (Table 1, green). Two genes were significantly downregulated upon exposure to VEGF but no significant change after removal of VEGF and significantly downregulated upon the reapplication of VEGF (Table 1, orange). Finally, six genes were significantly downregulated upon exposure to VEGF and then upregulated after removal of VEGF and then significantly downregulated upon the reapplication of VEGF (Fig. 3D, Table 1, purple). This data suggests that neural crest cell molecular profiles start to change in response to changes in VEGF within their surroundings in a matter of four minutes

Model migration efficiency depends on behavior-switching timescales

To explore the sensitivity of our model to the rates of switching between leader and trailer behavior, as implemented in the integrate-and-switch mechanism (Fig. 4A), we calculated the average number of cells in the domain at t = 24 hours, relative to the non-switching case , for different combinations of lead-to-follow and follow-to-lead switching times (Fig. 4B) Migration efficiency was higher when switching times were similar to each other (Fig. 4C). Outcome variability, measured as the coefficient of variation of cell number, was also lower for matched switching times (Fig. 4C). Migration was least efficient for slow follow-to-lead switching times (Fig. 4B). Together with the in vitro gene

expression analysis, which shows fast response to VEGF removal in particular (Fig. 3C) and thus suggests fast lead-to-follow switching, this constrains our model to behavior-switching timescales on the order of a few minutes.

Trailer neural crest cells respond to ectopic VEGF

We have previously shown that lead neural crest cells can respond and divert cell trajectories towards ectopic sources of VEGF placed adjacent to the migratory stream within typical cranial neural crest exclusion zones (McLennan et al., 2010). Our model simulations predict that trailing cells receive guidance instructions from leaders, rather than VEGF signals (McLennan, Dyson, et al., 2012). Thus, it has remained unclear whether trailing cells would respond or ignore an ectopic source of VEGF placed within or adjacent to the migratory stream. To address this, we waited until lead neural crest cells had migrated from the neural tube and placed ectopic sources of VEGF either adjacent to or within the trailing subpopulation of the stream (Fig. 1).

When an ectopic VEGF source was placed adjacent to the trailing subpopulation of the neural crest migratory stream, neural crest cells rerouted towards the VEGF source (Fig. 5B compared to 5A). Neither lead nor trailing neural crest cells were attracted to control cells transplanted into the same region (data not shown; McLennan et al, 2010). Static images suggested that neural crest cells originating from r3 and r4 diverted cell trajectories to move towards the ectopic VEGF-source (Fig. 5B). Time-lapse imaging confirmed this and revealed that r4 trailing neural crest cells in close proximity to the ectopic VEGF source (on the rostral portion of the stream); cells further away (caudal

portion of the stream appeared unaffected) (Fig. 6A, 6B, 6E; Movie 1). After encountering the perimeter of the ectopic VEGF source, some neural crest cells intermingled with the VEGF expressing cells (Fig. 6B).

In both time-lapse imaging and static analyses we saw a small number of trailing neural crest cells leave the migratory stream in response to VEGF (Fig. 5G). However, neural crest cells that remained in the migratory route clustered near the ectopic VEGF-source (Fig. 6B; Movie 1). The width of the stream was significantly increased when ectopic VEGF was placed adjacent to the trailing portion of the stream (Fig. 5H). Neural crest cells still migrated the entire length of the migratory route; hence the migration of the lead neural crest cell subpopulation was unaffected (Fig. 5B). High resolution time-lapses of neural crest cells prelabeled with a membrane marker showed that trailing neural crest cells remained reasonably immobile within the proximal portion of the stream while sending multiple filopodial protrusions towards the ectopic VEGF (Movie 2).

To determine whether trailing neural crest cells would respond to changes in VEGF signals after receiving instructions from leaders, we placed an ectopic VEGF source within the trailing subpopulation of cells (Fig. 6C, 5C compared to 5A). We found the trailing neural crest cells clustered around the ectopic VEGF source on both the proximal and distal sides of the source (Fig. 5C, 6D, 6F; Movie 3). We also found this increased the width of the neural crest migratory stream at the transplant site, and this

was not due to cells moving around the tissue transplant as a barrier, since some migrating neural crest cells could be observed to be within the transplant (Movie 4).

When the transplant was placed within the trailing portion of the stream, the width of the stream was wider at the transplant site compared to control streams (Fig. 5H). Furthermore, lead neural crest cells were still able to migrate normally the entire length of the migratory route (Fig. 5C). These results reveal that trailing neural crest cells can respond to VEGF, but prefer to remain within their comfort zone of the migratory stream if possible.

Altering the chemoattractant-distribution in model simulations causes break-up of the migratory stream

To test whether the observed effects of transplanting ectopic VEGF could be explained by our model with the integrate-and-switch mechanism, we computationally represented the tissue transplantation experiments (Fig. 5D-F). In the region of increased chemoattractant production, model simulations showed that trailing cells increasingly switched to become leader cells compared to the control simulations (Fig. 5E,F). This clustering of cells around the transplants resulted in a break-up of the stream into a distal-moving subpopulation and interacting with the ectopic chemoattractant (Fig. 5E,F,I). Thus, the effects of perturbing the VEGF distribution in vivo are consistent with our hypothesis of follow-the-leader migration in a cell-induced gradient with VEGF-induced cell behavior switching.

Trailer neural crest cells near ectopic sources of VEGF upregulate genes associated with the invasive front

To determine whether the trailing neural crest cells that responded to ectopic sources of VEGF changed their gene expression, we examined cells in physical contact with the ectopic sources of VEGF (Fig. 7A). Euclidean clustering did reveal that neural crest cells in contact with an ectopic source of VEGF placed within the trailing subregion of the migratory stream were most similar to wildtype trailing neural crest cells (Fig. 7B,C), with a dissimilarity score of 5.95 (Fig. 7C). We found there was a significant upregulation in the expression of 9 genes in response to the presence of VEGF (Fig. 7D). This included the expression of 4 genes (CCR9, CXCR1, PKP2, and BAMBI) (Fig. 7D); all of which we previously determined to be upregulated in a specific subpopulation of lead neural crest cells we termed trailblazers (McLennan, Schumacher et al., 2015). Together, this suggested that neural crest cells that encountered an ectopic VEGF source placed within the trailing subpopulation upregulated a subset of lead cell genes, but for the most part retained similarity to trailing cells.

When neural crest cells diverted away from the typical migratory pathway to encounter an ectopic VEGF source placed adjacent to the stream, we found their gene expression profile changes (Fig. 7B,C). There were 22 genes that were significantly upregulated in the neural crest cells responding to VEGF (Fig. 7E). This list includes 8 genes (CCR9, CXCR1, PKP2, BAMBI, CXCR7, NOTCH1, EPHB1 and CTNNB1) that are in the molecular signature of the invasive front (Fig. 7E, purple). Thus, neural crest cells that

diverted away from the discrete stream to interact with an ectopic VEGF source had a higher number of lead genes induced and 4 of these genes were shared with cells that encountered VEGF within a stream.

Trailer neural crest migration is unaffected by a reduction in VEGF

Our hypothesis states that trailing neural crest cells do not require VEGF signaling for guidance, but receive guidance instructions from lead cells. To test this, we knocked down VEGF function in the ectoderm directly overlying only the trailing portion of the neural crest migratory stream using targeted VEGF morpholino (Fig. 8A). Knocking down VEGF in the surface ectoderm had no effect on the width of the trailing neural crest cell subpopulation when we compared the stream width to control embryos (Fig. 8A). Second, when we bound up soluble VEGF protein in the trailing mesoderm by injecting Np1-Fc into the tissue, we found no effect to the trailing neural crest subpopulation (Fig. 8B). These results indicated that VEGF is not required for proper migration of the trailing cell population.

Lead molecular profiles are altered after reduction in VEGF signaling

We have previously shown that Np1 siRNA transfected neural crest cells exhibited reduced migration to the branchial arch target site (McLennan and Kulesa, 2007). To determine whether a reduction in cellular VEGF signaling significantly influenced the molecular profile of lead neural crest cells, we electroporated neural crest cells with Np1 siRNA and isolated these cells for qPCR. We compared the molecular profiles of lead and trailing neural crest cells transfected with Np1 siRNA to lead, middle and trailing

neural crest cells transfected with control EGFP. We determined that lead Np1 siRNA neural crest cells were most similar in gene expression profile to neural crest cells positioned mid-stream with a euclidean dissimilarity score of 7.70 (Fig. 9A,C). Trailing Np1 siRNA neural crest cells were most similar to trailing control neural crest cells with a euclidean dissimilarity score of 6.85 (Fig. 9A,C).

When we knocked down available VEGF by binding up endogenous VEGF with Np1-Fc injections into and around the migratory stream, we found that lead Np1-Fc neural crest cells were most similar to lead control neural crest cells with a euclidean dissimilarity score of 6.48 (Fig. 9B,D). Trailing Np1-Fc neural crest cells were most similar to trailing control neural crest cells with a euclidean dissimilarity score of 7.69 (Fig. 9B,D).

Comparison of specific genes that were up-regulated or down-regulated in lead neural crest cells after VEGF signaling reduction revealed that lead Np-1 siRNA neural crest cells down-regulated only 2 genes; one of these was associated with the invasive migratory front (Fig. 9E). There were 11 up-regulated genes, 4 of which we have associated with the invasive migratory front (Fig. 9E). In comparison, Np1-Fc injections resulted in only 1 up-regulated gene and 8 down-regulated genes in lead cells, 4 of which are associated with the trailblazer signature (Fig. 9E). Together, this data shows that knockdown of VEGF signaling by two distinct methods altered the expression profile in lead neural crest cells in distinct ways suggesting different cell responses to loss of VEGF signaling.

Discussion

We used the chick embryo system and computational modeling to study the importance of VEGF during neural crest cell migration in the head. We demonstrated that distinct genotypes of lead and trailer neural crest cells do not exist in vitro. However, exposure to VEGF in culture caused an upregulation of a small subset of lead genes in the most invasive neural crest cells. Further, timed addition and removal of VEGF in culture showed neural crest gene expression profiles change within minutes and provided the basis for incorporation of an integrate and switch mechanism into our computational model. Model simulations predicted migration efficiency is influenced by lead-to-trailer behavior switching timescales. We also showed that presentation of ectopic VEGF sources to trailer cells altered cell trajectories and gene expression, consistent with in silico predictions, but loss of VEGF signals did not. We conclude that VEGF and other microenvironmental signals are critical to establish lead neural crest cells that readout guidance signals and instruct trailers to follow.

Signals within the in vivo microenvironment rather than the neural tube establish distinct lead and trailer neural crest cell molecular signatures in the head. By analyzing gene expression in cranial neural crest cells that emigrated from neural tube explant cultures (Fig. 1), we found no evidence of either a trailblazer (McLennan et al., 2015) or lead cell signature (McLennan et al., 2012). Rather, neural crest cell gene expression profiles were similar independent of the distance migrated in the culture dish (Fig. 1). mRNA expression analysis followed by quantitation of fluorescence signals in individual migrating neural crest cells confirmed the lack of expression of key genes previously

correlated with in vivo leaders (Fig. 1F,G). The only exception to this was Runx2 (upregulated in leaders) and FoxD3 (upregulated in trailers), suggesting the expression of these two genes may be endowed by signals within the neural tube (Fig. 1B-D).

Exposure of VEGF to neural tube explant cultures partially re-covered the expression of genes associated with in vivo lead neural crest cells, including three trailblazer genes (Fig. 2; Bambi, Notch1, and Nedd9). This suggested that VEGF may be one of the in vivo microenvironmental signals that establish a distinct lead neural crest cell molecular signature. Of these trailblazer genes, elevated expression of Nedd9 has been associated with metastatic activity in several aggressive cancers (Li et al., 2014 (Intl J Clin Exp Pathol); Zhang et al., 2014 (Med Oncolo); Wang et al., 2014 (Hum Pathol)). Nedd9 has been shown to be critical to cancer cell invasion by stimulating a cell's ability to undergo an epithelial-to-mesenchymal transition, attachment to the extracellular matrix and migratory speed, when analyzed in vitro (Zhong et al., 2014 (Mol Cancer Res); Jin et al., 2014 (Intl J Cancer)); Sima et al., 2013 (PlosOne)). Further studies of VEGF and the trailblazer genes, including Nedd9 may reveal the interplay between VEGF stimulation and the functional role of these genes in neural crest migration.

Our computational model included a phenotypic switch from lead to trailer cell, the simulations of which predicted cell migration efficiency is influenced by switching timescales. By analyzing gene expression dynamics after timed addition and removal of VEGF in vitro, we observed a rapid and significant change in neural crest cell gene expression within 4 minutes (Figs. 3,4). From this data, we formulated a model

mechanism in silico by which lead cells become trailers after leaders fail to readout an appropriate level of VEGF over a short number of time steps. Simulations of the integrate and switch mechanism identified two model features that made migration more robust to perturbations (such as random variation in the directional cue provided by the chemoattractant): (1) a non-zero timescale of switching between leader and trailer cell states, and (2) hysteresis, or a memory, which decays with time, of the signal sensed (the directional cue). Thus, the integrate-and-switch mechanism, as presented here, provided the simplest extension to our existing model that captured the plasticity of neural crest cell behavioral identity and did so robustly. It is important to note that the integrate-and-switch mechanism in fact makes our model of neural crest cell migration less complex, in the sense that the size of the lead subpopulation does not need to be pre-specified, but emerges from the interactions of the cells with the chemoattractant distribution.

Trailer neural crest cells altered trajectories and gene expression in response to an ectopic source of VEGF, suggesting a trailer phenotype/genotype is not hard-wired. When ectopic VEGF was placed adjacent to the trailer subpopulation (in the region adjacent to r3), some trailer neural crest cells diverted away from the stream towards the ectopic VEGF source (Fig. 6). Diverted trailer cells that encountered the ectopic VEGF source had significant changes in gene expression, including upregulation of 22 genes, 8/22 were trailblazer signature genes (Fig. 7).

Similarly, ectopic VEGF placed within the trailer subpopulation caused newly exiting cells to congregate around and distal cells to reverse direction to move back to the VEGF source (Fig. 6). Neural crest cells that encountered ectopic VEGF upregulated 9 genes typically associated with the invasive front, 4/9 were trailblazer signature genes (Fig. 7). Four trailblazer signature genes were commonly upregulated (Bambi, Ccr9, Cxcr1, Pkp2) in the ectopic VEGF source transplantations. Chemokine receptors, Ccr9 and Cxcr1 have been implicated in aggressive cancers (Johnson-Holiday et al., 2011; Heinrich et al., 2013; Amersi et al., 2008), suggesting correlation with an invasive cell type. VEGF directly stimulated the expression of Cxcr1 and Ccr9 in trailer cells in response to ectopic VEGF (Fig. 7), but not in the presence of VEGF in vitro (Fig. 2). Whether the upregulation of Cxcr1 in trailer neural crest cells in response to ectopic VEGF also suggests the presence of the ligand IL8 is not known. The Cxcr1/Il8 axis has been implicated in a number of invasive cell migration events including mesenchymal stem cell migration to gliomas (Chen et al., 2014) and in neutrophil chemotaxis (Oehlers et al., 2010).

Model simulations predicted that neural crest cells that diverted towards ectopic VEGF sources switched from trailers to leaders, resulting in alterations to stream morphology that agreed with experimental results (Fig. 5). When VEGF was knocked down in either the ectoderm overlaying the trailing portion of the stream (reduce VEGF production) or the mesoderm (bind up existing VEGF protein), there was no effect on trailer neural crest cell migration (Fig. 8). This suggested that VEGF signals are not required for

guidance of trailer neural crest cells. Alternatively, trailer cell guidance may rely on other unknown microenvironmental signals.

In summary, our findings identify the importance of VEGF as one of the in vivo microenvironmental signals that establish a distinct subpopulation of lead neural crest cells. VEGF signals do not provide guidance cues to trailer neural crest cells, but convert trailers to lead cells that alter cell trajectories and gene expression when a VEGF source is introduced ectopically. This data supports our cell-induced gradient model that microenvironmental signals define and direct lead neural crest cells that instruct trailers to follow. Inclusion of an integrate and switch mechanism in silico, through which lead neural crest cells become trailers and vice-versa has a distinct timescale of switching to promote model migration efficiency. Together, these steps appear essential to promote neural crest cell persistence and stream cohesion. Further analysis of the cell behaviors and gene expression changes in neural crest cells that respond to ectopic VEGF sources may help to identify other microenvironmental guidance signals and the mechanistic underpinnings by which lead cells instruct trailers to follow.

Acknowledgements: PMK would like to acknowledge the kind and generous funding from the Stowers Institute for Medical Research. We also thank members of the BioInformatics, Histology and Molecular Biology core facilities at the Stowers Institute for Medical Research. Fluidigm Biomark HD dynamic arrays were analyzed at the Children's Hospital Boston IDDRC Molecular Genetics facility.

ADAM10	ITGA9
CDH2	ITGB1
CDH7	NOTCH1
COL2A1	NRP1
ERBB2	NRP2
FGFR1	PCDH1
FOXD3	ROBO1
ITGA4	SPON1
ITGA6	TGFBR1

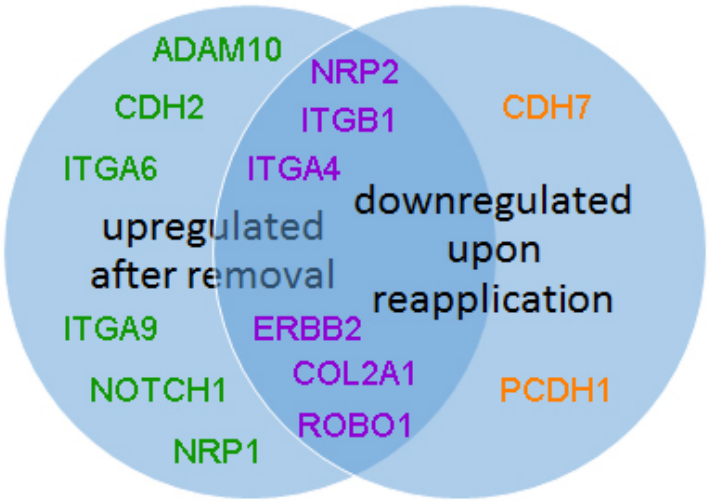

Table 1: Genes downregulated upon initial exposure to VEGF in vitro. Green genes were significantly downregulated upon exposure to VEGF and then upregulated after removal of VEGF but no significant change upon the reapplication of VEGF. Orange genes were significantly downregulated upon exposure to VEGF but no significant change after removal of VEGF and significantly downregulated upon the reapplication of VEGF. Purple genes were significantly downregulated upon exposure to VEGF and then upregulated after removal of VEGF and then significantly downregulated upon the reapplication of VEGF.

References

Alfandari, D., Cousin, H. and Marsden, M. (2010). Mechanism of Xenopus cranial neural crest cell migration. *Cell Adh Migr* **4**, 553-60.

Bron, R., Eickholt, B. J., Vermeren, M., Fragale, N. and Cohen, J. (2004). Functional knockdown of neuropilin-1 in the developing chick nervous system by siRNA hairpins phenocopies genetic ablation in the mouse. *Dev Dyn* **230**, 299-308.

Chapman, S. C., Collignon, J., Schoenwolf, G. C. and Lumsden, A. (2001). Improved method for chick whole-embryo culture using a filter paper carrier. *Dev Dyn* **220**, 284-9.

Clay, M. R. and Halloran, M. C. (2010). Control of neural crest cell behavior and migration: Insights from live imaging. *Cell Adh Migr* **4**, 586-94.

Gammill, L. S. and Roffers-Agarwal, J. (2010). Division of labor during trunk neural crest development. *Dev Biol* **344**, 555-65.

Hamburger, V. and Hamilton, H. L. (1951). A series of normal stages in the development of the chick embryo. *J Morphol* **88**, 49-92.

Kirby, M. L. and Hutson, M. R. (2010). Factors controlling cardiac neural crest cell migration. *Cell Adh Migr* **4**, 609-21.

Klymkowsky, M. W., Rossi, C. C. and Artinger, K. B. (2010). Mechanisms driving neural crest induction and migration in the zebrafish and Xenopus laevis. *Cell Adh Migr* **4**, 595-608.

Kulesa, P. M., Bailey, C. M., Kasemeier-Kulesa, J. C. and McLennan, R. (2010). Cranial neural crest migration: new rules for an old road. *Dev Biol* **344**, 543-54.

Kulesa, P. M. and Gammill, L. S. (2010). Neural crest migration: patterns, phases and signals. *Dev Biol* **344**, 566-8.

Lake, J. I. and Heuckeroth, R. O. (2013). Enteric nervous system development: migration, differentiation, and disease. *Am J Physiol Gastrointest Liver Physiol* **305**, G1-24.

McKinney, M. C., Fukatsu, K., Morrison, J., McLennan, R., Bronner, M. E. and Kulesa, P. M. (2013). Evidence for dynamic rearrangements but lack of fate or position restrictions in premigratory avian trunk neural crest. *Development* **140**, 820-30.

McLennan, R., Dyson, L., Prather, K. W., Morrison, J. A., Baker, R. E., Maini, P. K. and Kulesa, P. M. (2012). Multiscale mechanisms of cell migration during development: theory and experiment. *Development* **139**, 2935-44.

McLennan, R. and Kulesa, P. M. (2007). In vivo analysis reveals a critical role for neuropilin-1 in cranial neural crest cell migration in chick. *Dev Biol* **301**, 227-39.

McLennan, R., Teddy, J. M., Kasemeier-Kulesa, J. C., Romine, M. H. and Kulesa, P. M. (2010). Vascular endothelial growth factor (VEGF) regulates cranial neural crest migration in vivo. *Dev Biol* **339**, 114-25.

Newgreen, D. F., Dufour, S., Howard, M. J. and Landman, K. A. (2013). Simple rules for a "simple" nervous system? Molecular and biomathematical approaches to enteric nervous system formation and malformation. *Dev Biol* **382**, 305-19.

Perris, R. and Perissinotto, D. (2000). Role of the extracellular matrix during neural crest cell migration. *Mech Dev* **95**, 3-21.

Powell, D. R., Blasky, A. J., Britt, S. G. and Artinger, K. B. (2013). Riding the crest of the wave: parallels between the neural crest and cancer in epithelial-to-mesenchymal transition and migration. *Wiley Interdiscip Rev Syst Biol Med* **5**, 511-22.

Prud'homme, G. J. and Glinka, Y. (2012). Neuropilins are multifunctional coreceptors involved in tumor initiation, growth, metastasis and immunity. *Oncotarget* **3**, 921-39.

Teddy, J. M. and Kulesa, P. M. (2004). In vivo evidence for short- and long-range cell communication in cranial neural crest cells. *Development* **131**, 6141-51.

Theveneau, E. and Mayor, R. (2012). Neural crest migration: interplay between chemorepellents, chemoattractants, contact inhibition, epithelial-mesenchymal transition, and collective cell migration. *Wiley Interdiscip Rev Dev Biol* **1**, 435-45.
Uriu, K., Morelli, L. G. and Oates, A. C. (2014). Interplay between intercellular signaling and cell movement in development. *Semin Cell Dev Biol*.

Figure Legends

Figure 1: Neural crest cells do not maintain lead and trailing molecular profiles in vitro. (A) Schematic of in vitro and in vivo neural crest isolation from proximal and distal regions. (B-C) Euclidean clustering and euclidean dissimilarity matrix plot of proximal and distal molecular profiles isolated from in vitro and in vivo samples. (D) Venn diagram of genes significantly upregulated in distal neural crest cells. (E) Venn diagram of genes significantly upregulated in proximal neural crest cells. (F) HCR of neural crest cells grown in vitro, probed for FOXD3, HAND2 and BAMBI. (G) Mean fluorescence intensity of the HCR probes. Nt, neural tube, r4, rhomobomere 4, 24h, 24 hours, LCM, laser capture microdissection, RTqPCR, reverse transcription quantitative polymerase chain reaction, FL, fluorescence.

Figure 2: Neural crest cells upregulate genes typically associated with the migratory invasive front when exposed to VEGF. (A) Schematic of experimental design. (B, C) Euclidean clustering and euclidean dissimilarity matrix plot of distal and proximal molecular profiles isolated from in vitro after addition of VEGF and in vivo samples. (D) Genes significantly upregulated and downregulated in distal in vitro neural crest cells upon exposure to VEGF compared to lead neural crest cells in vivo. Purple highlight indicates genes typically associated with the neural crest cell trailblazers. Nt, neural tube, r4, rhombomere 4, 24h, 24 hours, LCM, laser capture microdissection, RTqPCR, reverse transcription quantitative polymerase chain reaction.

Figure 3: Response of neural crest cell molecular profiles to VEGF. (A) Experimental time-course. (B) Individual and average response (weighted by the inverse error in the mean) of genes with significant ($p<0.1$) and consistent (repeated across three experimental conditions) differential expression. Error bars show weighted

sample deviation. (C) Summary of first response times of genes after removal and readdition of VEGF. (D) Relative changes in expression of genes responding within four minutes under both conditions. R4, rhombomere 4, nt, neural tube

Figure 4: Model migration efficiency is influenced by behavior-switching timescales. (A) Schematic of integrate-and-switch model for leader-trailer transitions. (B) Effect of switching times on model migration efficiency (defined as the average number of cells after t = 24 hours (n=20 simulations), relative to the maximum for the non-switching case (as in McLennan, Schumacher et al). Point spacing indicates parameter combinations sampled. White contours show >15% coefficient of variation, grey contours >20%. (C) Migration efficiency (solid lines) and coefficient of variation (dashed lines) as a function of the ratio of switching times.

Figure 5: Trailing neural crest cells respond to VEGF in vivo. (A) Cranial neural crest stream labeled with DiO (green) (n=18 embryos). (B) VEGF-expressing cells (red) were transplanted adjacent to trailing portion of the cranial neural crest stream (green) (n=12 embryos). (C) Ectopic VEGF cell transplant (red) placed within the trailing portion of the cranial neural crest stream (green) (n=11 embryos). (D) Representative control model simulation. (E) Representative model simulation with increased chemoattractant production at bottom left edge of domain from t=12 hours onwards. (F) Representative model simulation with increased chemoattractant production at bottom left area from t=12 hours onwards. (G) Average number of neural crest cells found in area adjacent to r3. *Need to add back p values to graph* (H) Width of the stream at the transplant. (I) Migration profiles of control and perturbed simulations, averaged over n=20 simulations.

Figure 6: Trailing neural crest cells reroute towards VEGF in vivo. (A, C) Schematic representations showing placement of the VEGF-expressing cells. (B) Selected images from a typical time-lapse imaging session showing neural crest cells responding to VEGF-expressing cells (red) transplanted adjacent to the trailing stream

(green). *Sentence about the circles around some of the neural crest.* (D) Selected images from a typical time-lapse imaging session showing neural crest cells responding to VEGF-expressing cells (red) transplanted within the trailing stream (green). (E) Examples of neural crest cell tracks in response to VEGF from timelapse shown in B. (F) Examples of neural crest cell tracks in response to VEGF from timelapse shown in D. r4, rhombomere 4.

Figure 7: Trailing neural crest upregulate trailblazer genes in response to VEGF. (A) Schematic representation of the experiment. (B-C) Euclidean clustering and Euclidean dissimilarity matrix plot of neural crest cells responding to VEGF. (D, E) Genes significantly upregulated in response to VEGF placed within (D) and adjacent (E). Purple highlight indicates genes typically associated with the neural crest cell trailblazers.

Figure 8: Trailing neural crest cell migration is not dependent on VEGF. (A) Schematic representation of experimental design of transfecting ectoderm with VEGF morpholino, transverse section of the trailing neural crest migratory stream (green) with VEGF morpholino electroporated into the overlaying ectoderm (red), width of the trailing portion of the migratory stream after ectoderm transfections. (B) Schematic representation of experimental design of injecting Np1-Fc into the trailing mesenchyme, transverse section of the trailing neural crest migratory stream (green) after Np1-Fc injection, width of the trailing portion of the migratory stream after Np1-Fc injections. R4, rhombomere 4, MO, morpholino.

Figure 9: Lead neural crest cells change their molecular profiles in response to perturbed VEGF signaling. (A, C) Euclidean clustering and Euclidean dissimilarity matrix plot of neural crest cells transfected with Np1 siRNA. (B, D) Euclidean clustering and Euclidean dissimilarity matrix plot of neural crest cells after Np1-Fc injections. (E)Genes significantly altered after VEGF signaling perturbations. Purple highlight indicates genes typically associated with the neural crest cell trailblazers.

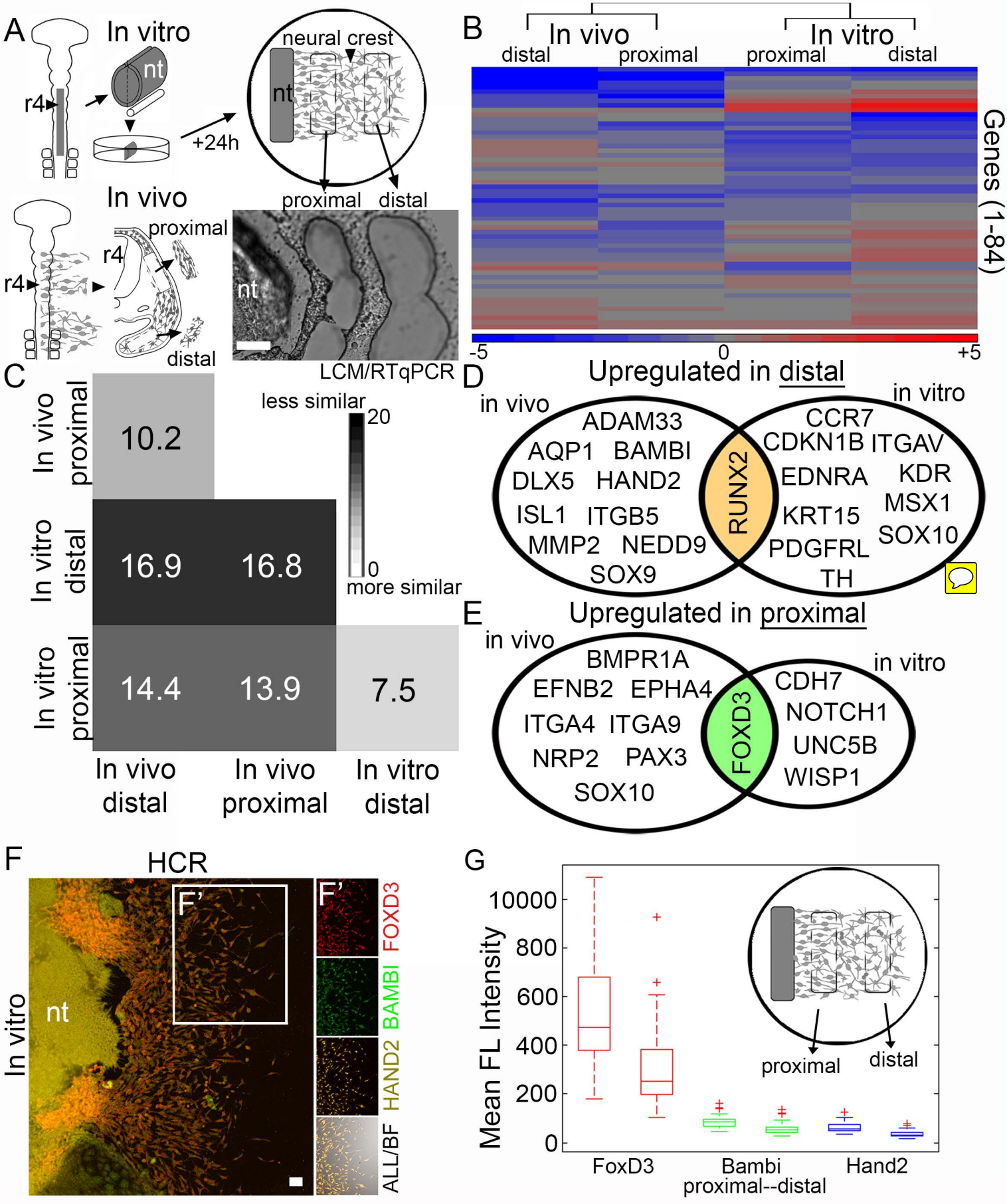
A
In vitro
r4
nt
+24h
neural crest
nt
proximal
distal
In vivo
r4
proximal
distal
nt
LCM/RTqPCR
B
In vivo
In vitro
distal
proximal
proximal
distal
Genes (1-84)
-5
0
+5
C
less similar
20
0
more similar
In vivo proximal
In vitro distal
In vitro proximal
10.2
16.9
16.8
14.4
13.9
7.5
In vivo distal
In vivo proximal
In vitro distal
D
Upregulated in distal
in vivo
in vitro
ADAM33
AQP1
BAMBI
DLX5
HAND2
ISL1
ITGB5
MMP2
NEDD9
SOX9
RUNX2
CCR7
CDKN1B
ITGAV
EDNRA
KDR
MSX1
KRT15
SOX10
PDGFRL
TH
E
Upregulated in proximal
in vivo
in vitro
BMPR1A
EFNB2
EPHA4
ITGA4
ITGA9
NRP2
PAX3
SOX10
FOXD3
CDH7
NOTCH1
UNC5B
WISP1
F
HCR
In vitro
nt
F'
F'
FOXD3
BAMBI
HAND2
ALL/BF
G
Mean FL Intensity
10000
800
600
400
200
0
proximal
distal
FoxD3
Bambi
Hand2
proximal--distal

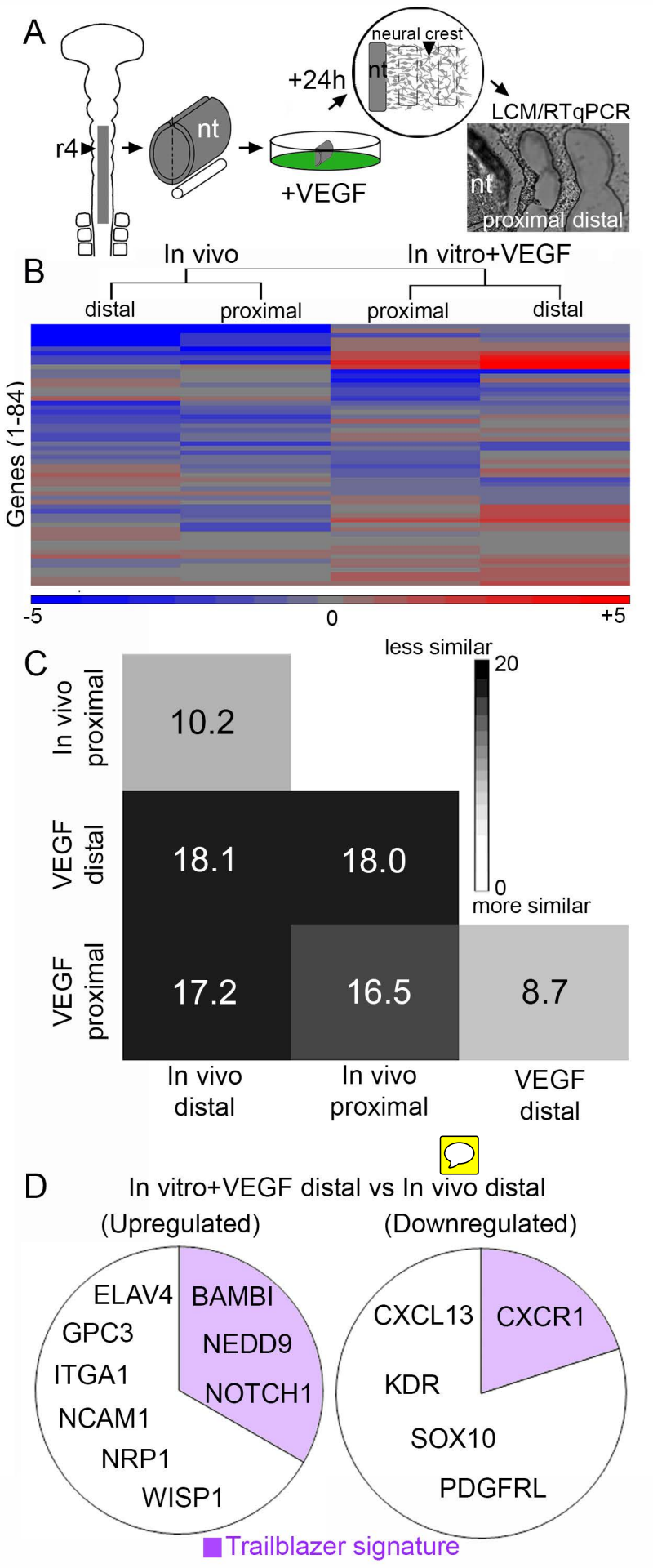
A
r4
nt
+VEGF
+24h
neural crest
nt
LCM/RTqPCR
nt
proximal distal
B
In vivo
In vitro+VEGF
distal
proximal
proximal
distal
Genes (1-84)
-5
0
+5
C
less similar
20
0
more similar
In vivo proximal
VEGF distal
VEGF proximal
10.2
18.1
18.0
17.2
16.5
8.7
In vivo distal
In vivo proximal
VEGF distal
D
In vitro+VEGF distal vs In vivo distal
(Upregulated)
(Downregulated)
ELAV4
GPC3
ITGA1
NCAM1
NRP1
WISP1
BAMBI
NEDD9
NOTCH1
CXCL13
KDR
SOX10
PDGFRL
CXCR1
Trailblazer signature

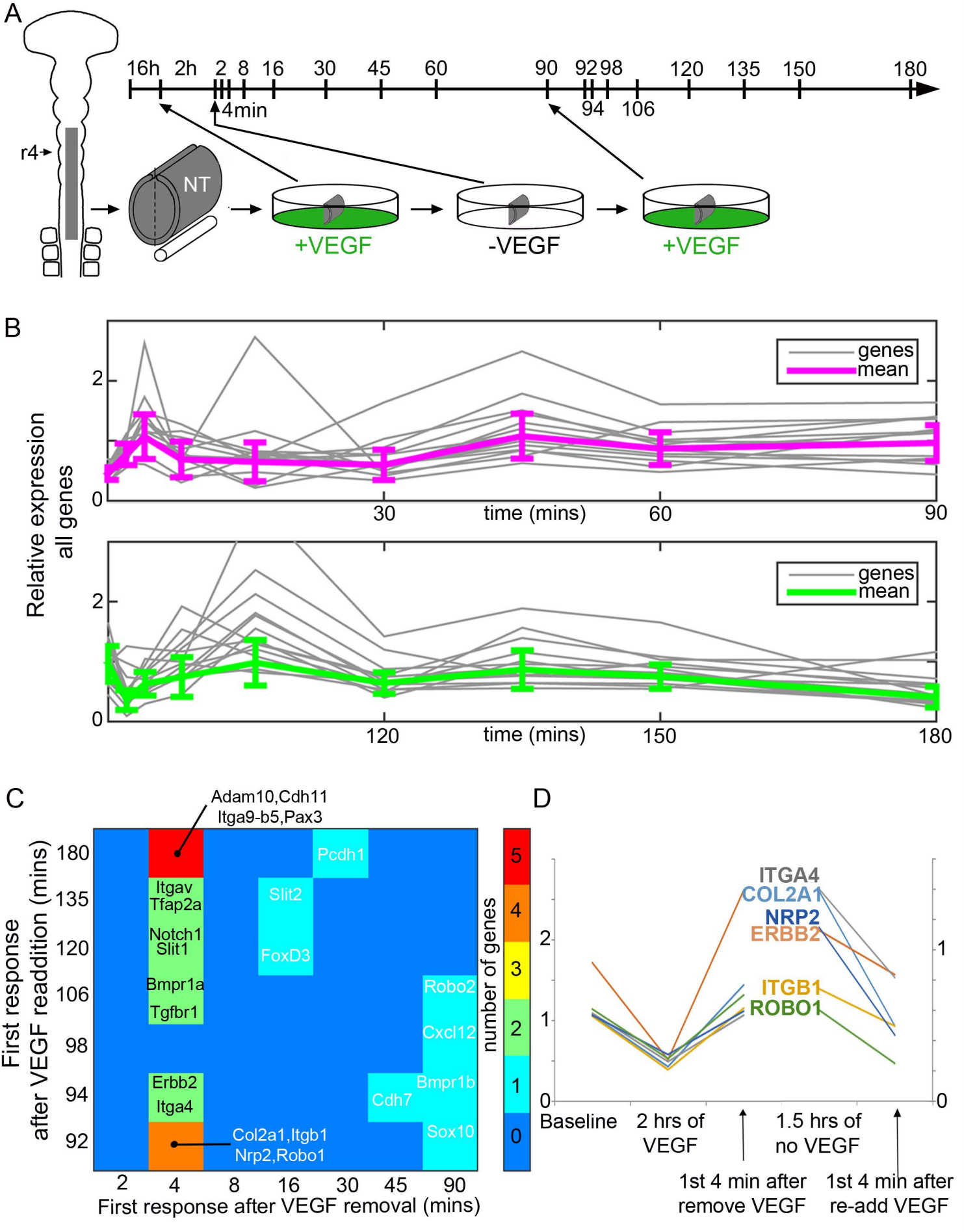
A
16h 2h 2 8 16 30 45 60 90 92 98 120 135 150 180
4min
94 106
r4
NT
+VEGF
-VEGF
+VEGF
B
Relative expression
all genes
genes
mean
time (mins)
C
Adam10,Cdh11
Itga9-b5,Pax3
Pcdh1
Itgav
Tfap2a
Slit2
Notch1
Slit1
FoxD3
Bmpr1a
Tgfbr1
Robo2
Cxcl12
Erbb2
Itga4
Bmpr1b
Cdh7
Sox10
Col2a1,Itgb1
Nrp2,Robo1
First response
after VEGF readdition (mins)
First response after VEGF removal (mins)
number of genes
D
ITGA4
COL2A1
NRP2
ERBB2
ITGB1
ROBO1
Baseline
2 hrs of
VEGF
1.5 hrs of
no VEGF
1st 4 min after
remove VEGF
1st 4 min after
re-add VEGF

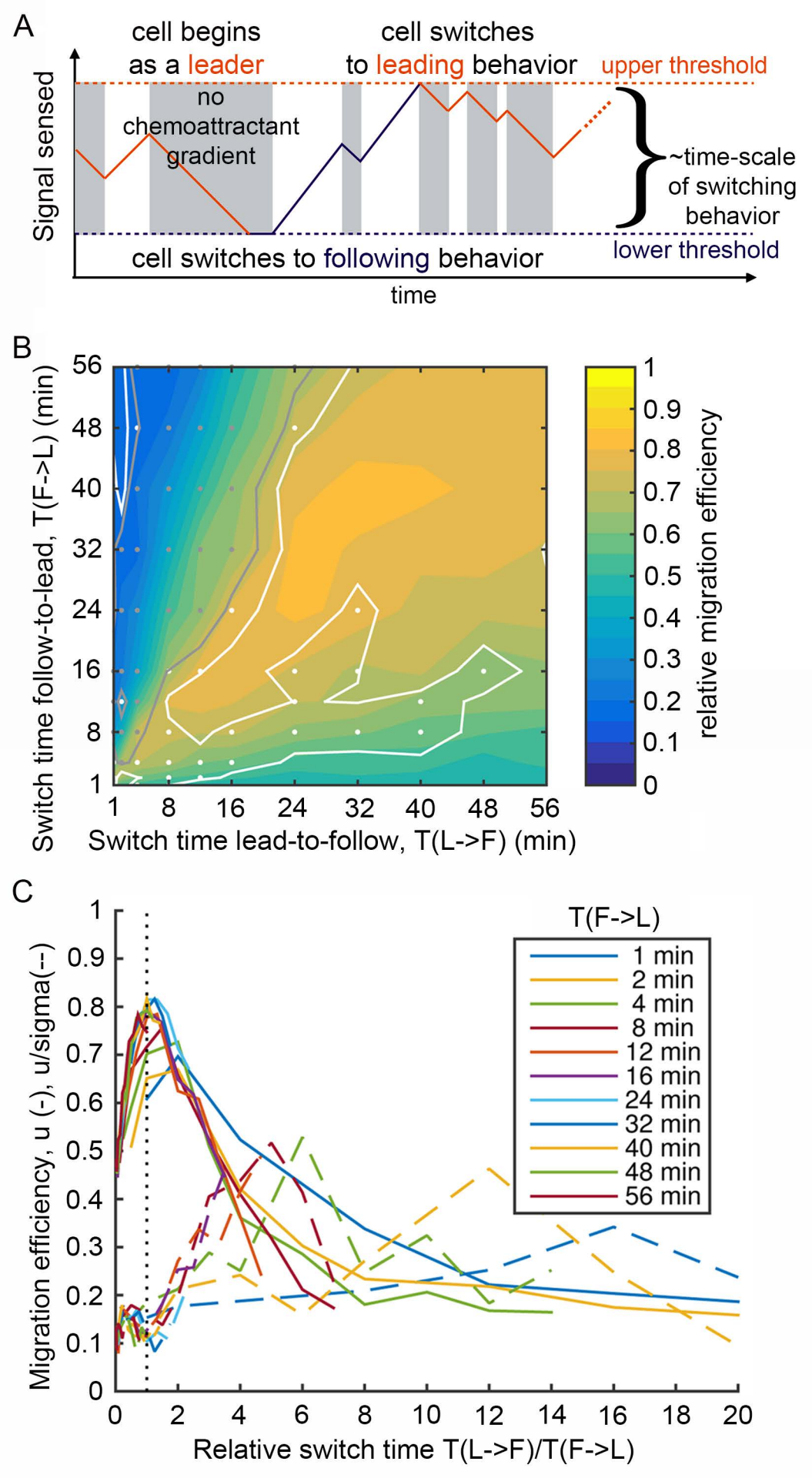
A
cell begins as a leader
cell switches to leading behavior
upper threshold
no chemoattractant gradient
Signal sensed
~time-scale of switching behavior
cell switches to following behavior
lower threshold
time
B
Switch time follow-to-lead, T(F->L) (min)
Switch time lead-to-follow, T(L->F) (min)
relative migration efficiency
C
Migration efficiency, u (-), u/sigma(--)
Relative switch time T(L->F)/T(F->L)
T(F->L)
1 min
2 min
4 min
8 min
12 min
16 min
24 min
32 min
40 min
48 min
56 min

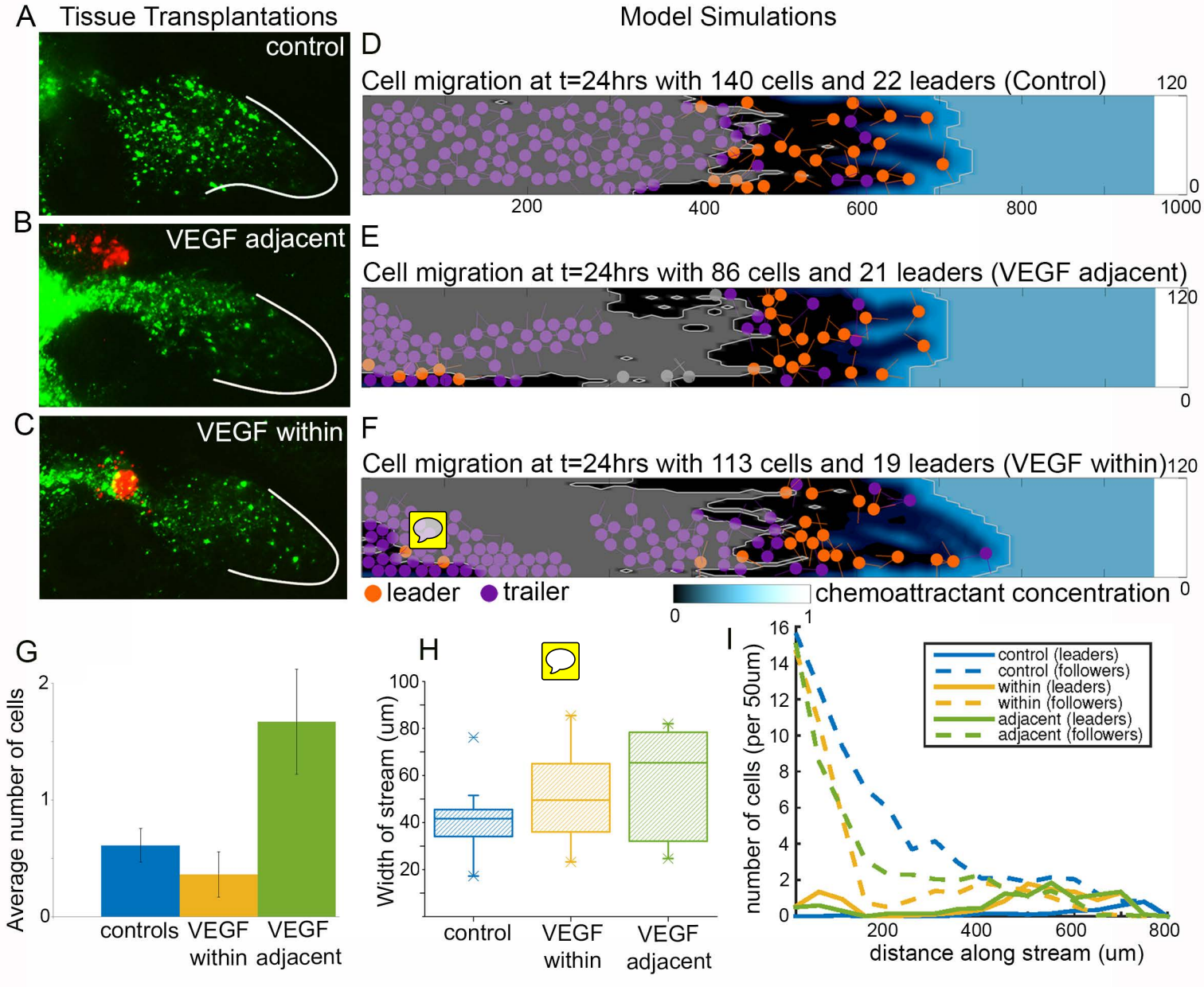
A
Tissue Transplantations
control
B
VEGF adjacent
C
VEGF within
Model Simulations
D
Cell migration at t=24hrs with 140 cells and 22 leaders (Control)
120
0
200
400
600
800
1000
E
Cell migration at t=24hrs with 86 cells and 21 leaders (VEGF adjacent)
120
0
F
Cell migration at t=24hrs with 113 cells and 19 leaders (VEGF within)
120
0
leader
trailer
chemoattractant concentration
0
1
G
Average number of cells
2
1
0
controls
VEGF within
VEGF adjacent
H
Width of stream (um)
100
80
60
40
20
control
VEGF within
VEGF adjacent
I
number of cells (per 50um)
16
14
12
10
8
6
4
2
0
200
400
600
800
distance along stream (um)
control (leaders)
control (followers)
within (leaders)
within (followers)
adjacent (leaders)
adjacent (followers)

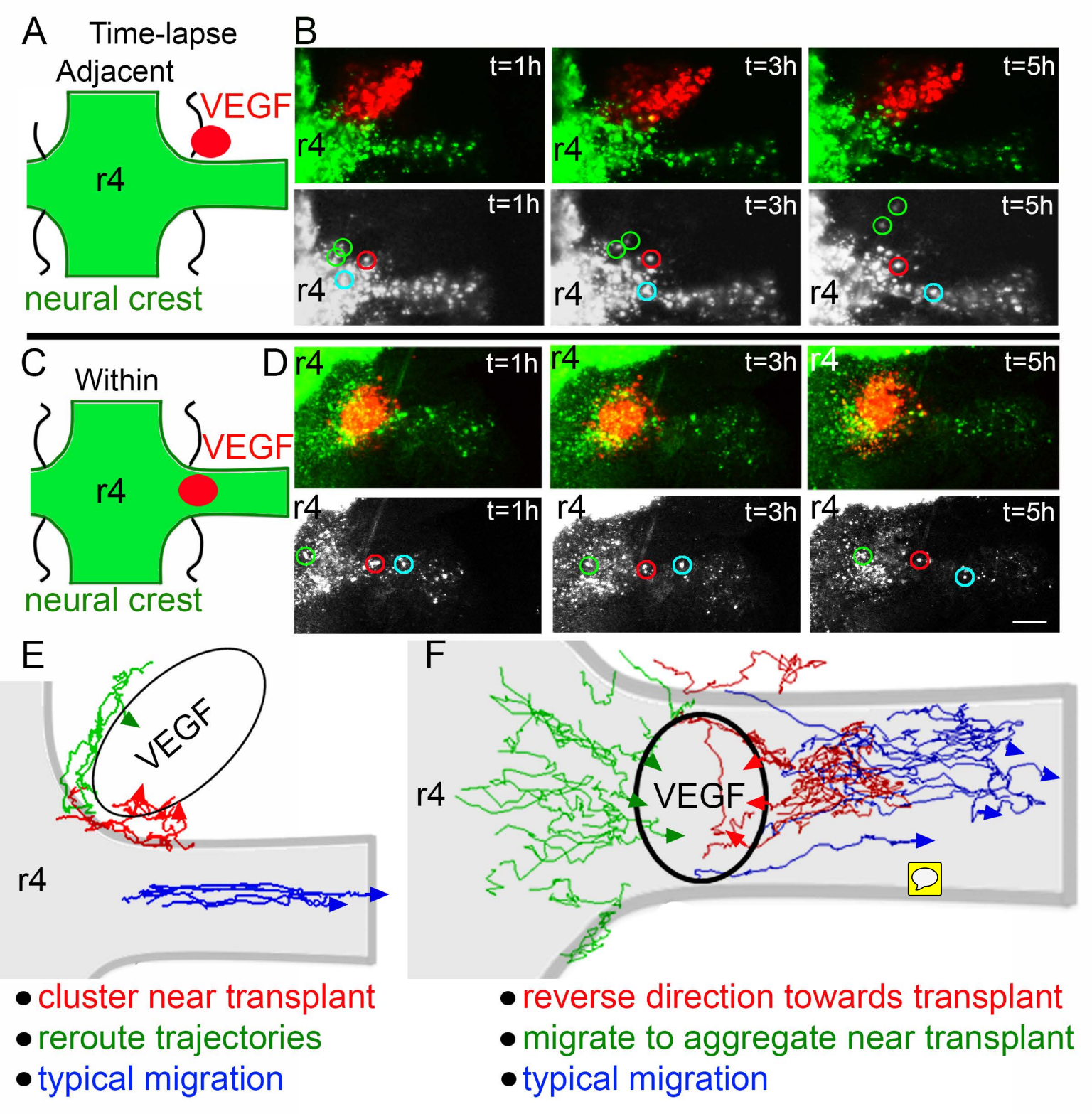
A
Time-lapse
Adjacent
VEGF
r4
neural crest
B
t=1h
t=3h
t=5h
r4
C
Within
VEGF
r4
neural crest
D
E
VEGF
r4
F
r4
VEGF
cluster near transplant
reroute trajectories
typical migration
reverse direction towards transplant
migrate to aggregate near transplant
typical migration

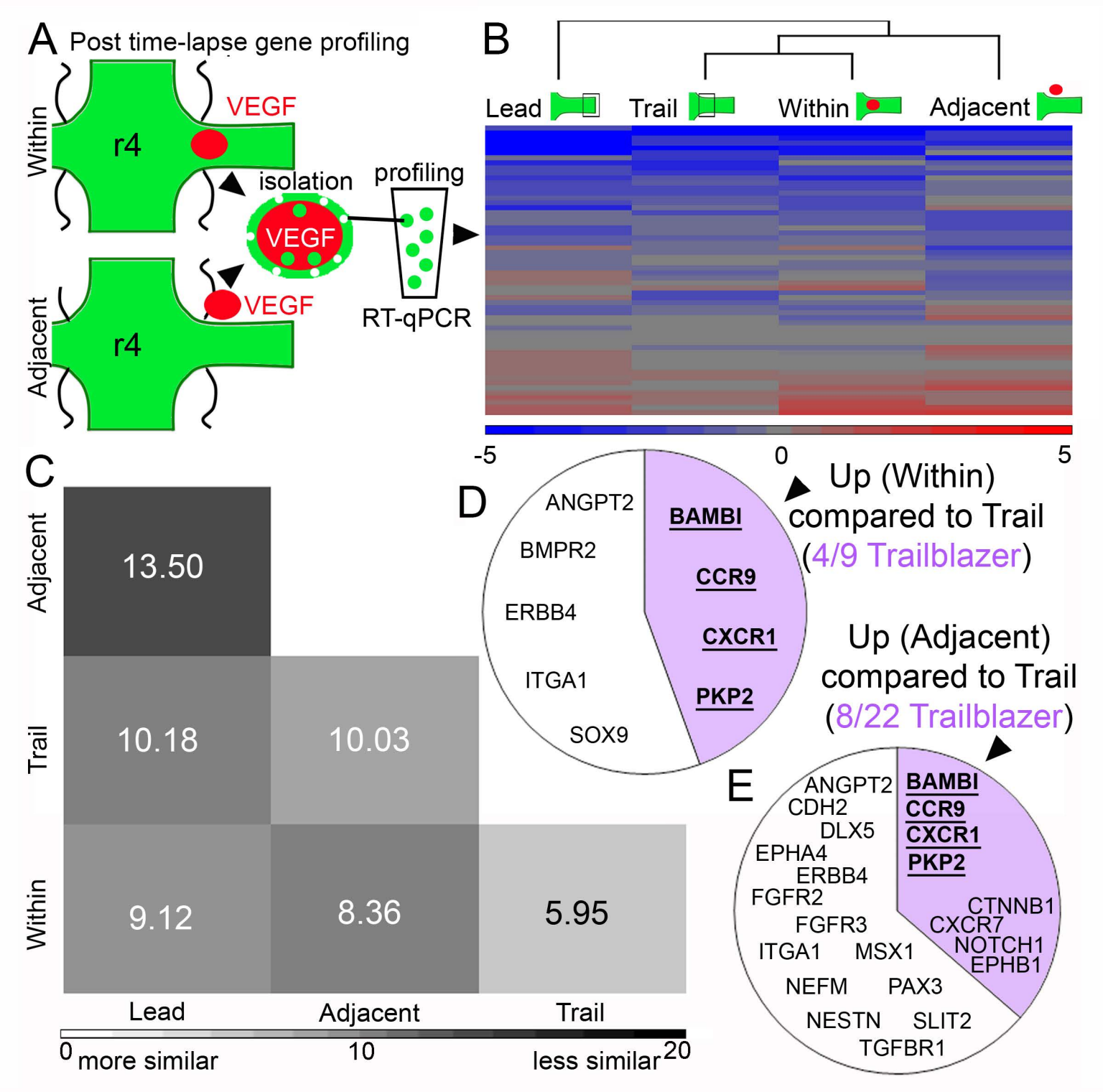
A
Post time-lapse gene profiling
Within
r4
VEGF
isolation
VEGF
profiling
RT-qPCR
Adjacent
r4
VEGF
B
Lead
Trail
Within
Adjacent
-5
0
5
C
Adjacent
Trail
Within
13.50
10.18
10.03
9.12
8.36
5.95
Lead
Adjacent
Trail
0 more similar
10
less similar 20
D
ANGPT2
BMPR2
ERBB4
ITGA1
SOX9
BAMBI
CCR9
CXCR1
PKP2
Up (Within) compared to Trail (4/9 Trailblazer)
Up (Adjacent) compared to Trail (8/22 Trailblazer)
E
ANGPT2
CDH2
DLX5
EPHA4
ERBB4
FGFR2
FGFR3
ITGA1
MSX1
NEFM
PAX3
NESTN
SLIT2
TGFBR1
BAMBI
CCR9
CXCR1
PKP2
CTNNB1
CXCR7
NOTCH1
EPHB1

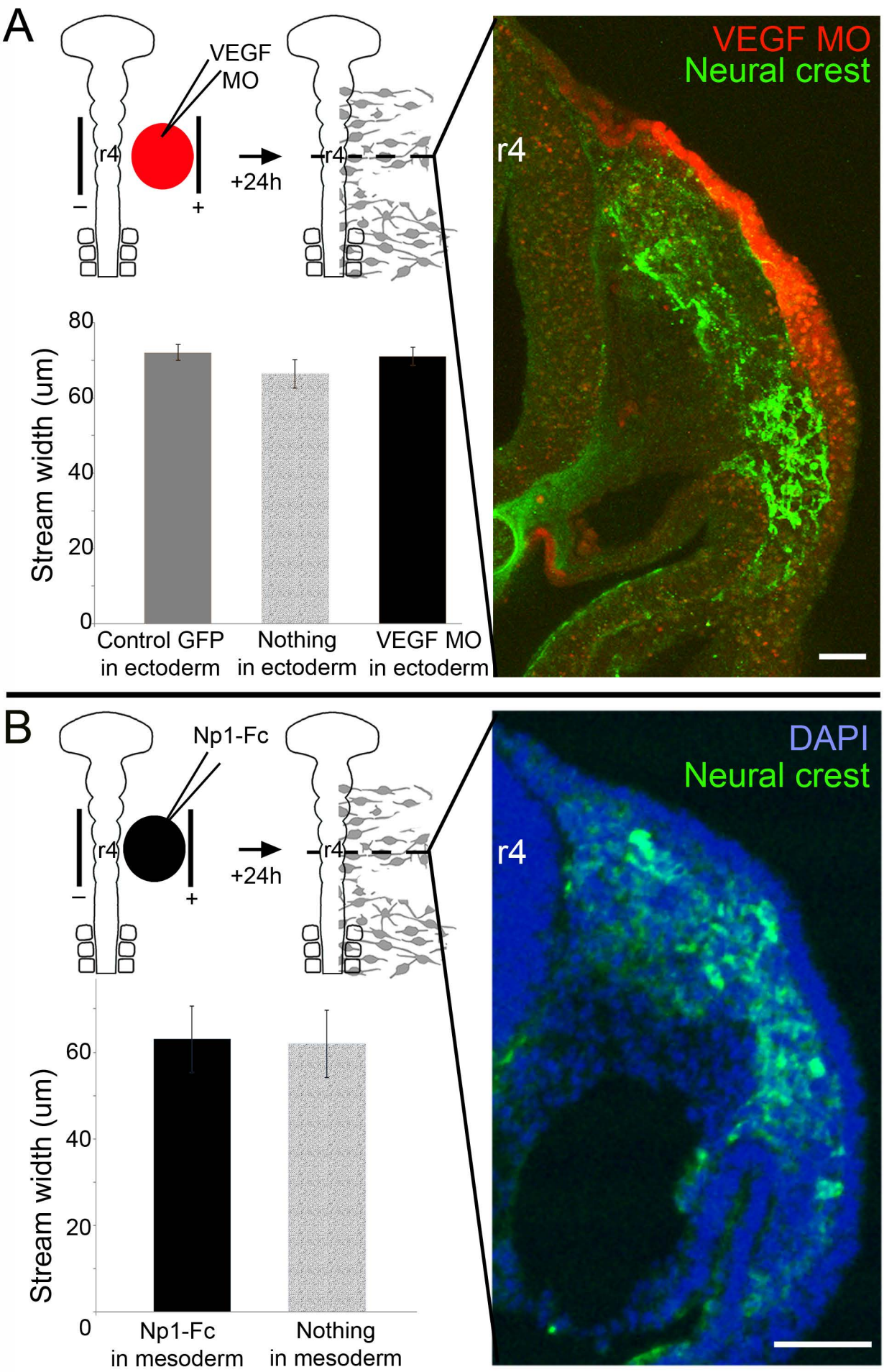
A
VEGF
MO
r4
+24h
r4
–
+
Stream width (um)
80
60
40
20
0
Control GFP
in ectoderm
Nothing
in ectoderm
VEGF MO
in ectoderm
VEGF MO
Neural crest
r4
B
Np1-Fc
r4
+24h
r4
–
+
Stream width (um)
60
40
20
0
Np1-Fc
in mesoderm
Nothing
in mesoderm
DAPI
Neural crest
r4

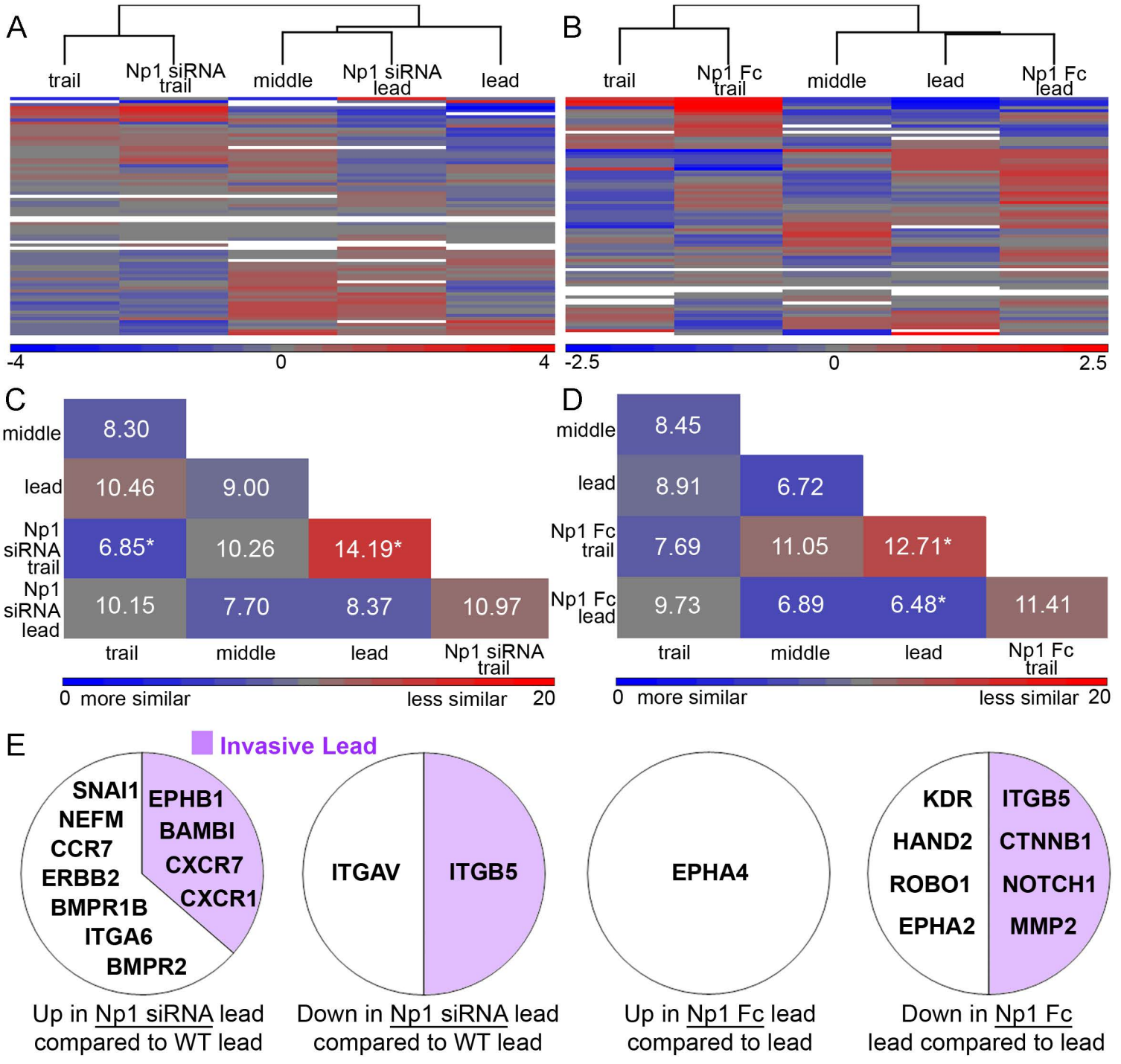
A
trail
Np1 siRNA trail
middle
Np1 siRNA lead
lead
-4
0
4
B
trail
Np1 Fc trail
middle
lead
Np1 Fc lead
-2.5
0
2.5
C
middle
lead
Np1 siRNA trail
Np1 siRNA lead
8.30
10.46
9.00
6.85*
10.26
14.19*
10.15
7.70
8.37
10.97
trail
middle
lead
Np1 siRNA trail
0 more similar
less similar 20
D
middle
lead
Np1 Fc trail
Np1 Fc lead
8.45
8.91
6.72
7.69
11.05
12.71*
9.73
6.89
6.48*
11.41
trail
middle
lead
Np1 Fc trail
0 more similar
less similar 20
E
Invasive Lead
SNAI1
NEFM
CCR7
ERBB2
BMPR1B
ITGA6
BMPR2
EPHB1
BAMBI
CXCR7
CXCR1
Up in Np1 siRNA lead compared to WT lead
ITGAV
ITGB5
Down in Np1 siRNA lead compared to WT lead
EPHA4
Up in Np1 Fc lead compared to lead
KDR
HAND2
ROBO1
EPHA2
ITGB5
CTNNB1
NOTCH1
MMP2
Down in Np1 Fc lead compared to lead